

# Near-Band-Edge Optical Responses of $\text{CH}_3\text{NH}_3\text{PbCl}_3$ Single Crystals: Photon Recycling of Excitonic Luminescence

Takumi Yamada, Tomoko Aharen, and Yoshihiko Kanemitsu\*  
*Institute for Chemical Research, Kyoto University, Uji, Kyoto 611-0011, Japan*



(Received 12 July 2017; published 1 February 2018)

The determination of the band gap and exciton energies of lead halide perovskites is very important from the viewpoint of fundamental physics and photonic device applications. By using photoluminescence excitation (PLE) spectra, we reveal the optical properties of  $\text{CH}_3\text{NH}_3\text{PbCl}_3$  single crystals in the near-band-edge energy regime. The one-photon PLE spectrum exhibits the 1s exciton peak at 3.11 eV. On the contrary, the two-photon PLE spectrum exhibits no peak structure. This indicates photon recycling of excitonic luminescence. By analyzing the spatial distribution of the excitons and photon recycling, we obtain 3.15 eV for the band gap energy and 41 meV for the exciton binding energy.

DOI: [10.1103/PhysRevLett.120.057404](https://doi.org/10.1103/PhysRevLett.120.057404)

The lead halide perovskites  $\text{MAPbX}_3$  ( $\text{MA} = \text{CH}_3\text{NH}_3$  and  $\text{X} = \text{I}, \text{Br}, \text{and Cl}$ ) are receiving considerable attention because they are cost effective and yet superior photovoltaic materials. Especially the solar cells based on  $\text{MAPbI}_3$  have experienced a rapid development because of its various advantageous properties such as a sharp absorption edge, high luminescence efficiency, low trap densities, and a long diffusion length [1–13]. In addition, by exchanging the halide component in  $\text{MAPbX}_3$ , the band gap can be tuned continuously over the whole visible spectral range [14–17]. Therefore, these perovskites are well suited for light-emitting devices (LEDs) and detectors in various wavelength regions [16–20].

The near-band-edge properties of these perovskites are important, because they are related to the solar cell and luminescence efficiencies. In addition, the possibility for the formation of band-tail states that are governed by the Rashba effect is under intense discussion [21,22]. Therefore, the accurate determination of the intrinsic near-band-edge optical properties is essential for future development. However, optical spectra of perovskite polycrystalline thin films are highly influenced by the grain size, surface roughness, and optical scattering of the incident light [23–27]. To eliminate extrinsic effects from the optical spectra, further experimental studies on perovskite single crystals with flat surfaces are needed.

In  $\text{MAPbI}_3$  and  $\text{MAPbBr}_3$  single crystals, the efficient band-to-band luminescence with no Stokes shift is strongly reabsorbed, and this leads to photon recycling, i.e., the

repetition between internal light emission and reabsorption [28–30]. In contrast, a very sharp peak appears in the absorption spectrum of the wide-gap semiconductor  $\text{MAPbCl}_3$  [31], which means that excitons dominate its optical properties even at room temperature, similar to other wide-gap semiconductors [32]. So far, photon recycling of excitonic luminescence has not been reported. This is because, in general, the room-temperature quantum efficiency of the excitonic luminescence is low in inorganic bulk crystals and a large luminescence Stokes shift appears in organic molecules. However, organic-inorganic hybrid perovskites exhibit efficient luminescence with no Stokes shift even at room temperature. The effect of the photon recycling of excitonic luminescence on the near-band-edge optical properties of  $\text{MAPbCl}_3$  needs to be clarified, because photon recycling has several advantages for optical devices [33–37].

In this Letter, the excitonic responses of  $\text{MAPbCl}_3$  single crystals are studied by one- and two-photon photoluminescence excitation (1- and 2-PLE) spectroscopy. By comparing the results obtained from one- and two-photon excitation, which provide information upon excitation of the near surface and the interior region of the sample, respectively, we can determine the intrinsic optical spectra of thick samples. The shape of the 1- and 2-PLE spectra clearly demonstrates that the PL spectrum of the optically thick single crystal is strongly influenced by the reabsorption of photons emitted from the inside. The obtained one-photon absorption spectra clearly show that  $\text{MAPbCl}_3$  is a direct-gap semiconductor and has no significant band-tail states. The analysis of the spatial distribution of the photoexcited carriers and the effect of reabsorption allowed us to deduce an accurate band gap energy of 3.15 eV and an exciton binding energy of 41 meV. The highly efficient luminescence in combination with no Stokes shift enables a strong photon recycling due to excitonic PL and absorption.

*Published by the American Physical Society under the terms of the Creative Commons Attribution 4.0 International license. Further distribution of this work must maintain attribution to the author(s) and the published article's title, journal citation, and DOI.*

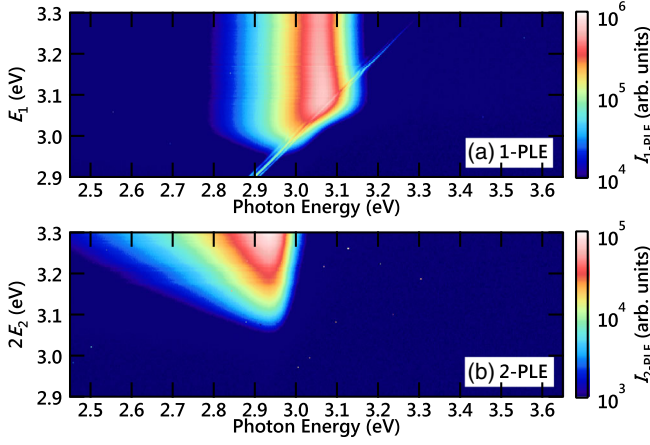


FIG. 1. (a) 1-PLE and (b) 2-PLE spectral maps for the MAPbCl<sub>3</sub> single crystal.  $E_1$  and  $E_2$  correspond to the excitation laser energy during 1- and 2-PLE measurements, respectively.

The optical experiments were performed on a MAPbCl<sub>3</sub> single crystal at room temperature. The details of sample preparation and experimental setup are given in Supplemental Material [38]. The two-dimensional (2D) 1- and 2-PLE spectral maps for the MAPbCl<sub>3</sub> single crystal are shown in Figs. 1(a) and 1(b), respectively.  $E_1$  corresponds to the excitation photon energy for the 1-PLE, and  $E_2$  corresponds to the photon energy for the 2-PLE. We note that the 2-PLE spectra have a different PL peak position compared with the 1-PLE spectra.

The comparison of the PL spectra obtained from single crystals and thin films clarifies the mechanism for the 1-PLE spectra within the range  $2.99 < E_1 < 3.11$  eV. The PL spectra obtained from Fig. 1(a) for five different excitation energies ( $E_1 = 2.99$ – $3.11$  eV) are shown with the red dots in Fig. 2(a). The photon energy is close to the band gap of the MAPbCl<sub>3</sub> single crystal, and one-photon absorption is dominant. The peculiar asymmetric shape of the PL spectrum is explained in Supplemental Material [38]. The PL spectrum of the thin film for  $E_1 = 3.50$  eV is shown with the blue line for comparison. The spectra obtained from the single crystal above  $E_1 = 3.11$  eV exhibited a peak at 3.06 eV and are almost equivalent with those of the thin film. On the other hand, when the excitation energy was tuned below 3.11 eV, the PL spectra experienced a redshift. Because the excitation light penetrates deep into the crystal for excitation energies within the energetic range of the PL spectrum, the spatial distribution of the photoexcited carriers has to be considered. In the case of optically thick single crystals, the internal luminescence is reabsorbed by the crystal itself [28–30]. Under one-photon excitation, the distribution of the photoexcited carriers can be expressed with [39]

$$n_1(z) = \frac{\alpha_1 I_1 \Delta t_1}{E_1} e^{-\alpha_1 z}. \quad (1)$$

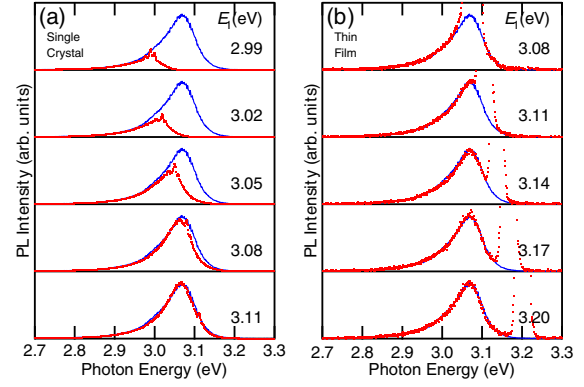


FIG. 2. The PL spectra (red data points) for (a) the single crystal and (b) the thin film, under one-photon excitation with energies close to the band edge of MAPbCl<sub>3</sub>. For comparison, the PL spectrum for an excitation of the thin film with  $E_1 = 3.50$  eV is shown with the blue curve.

Here,  $I_1$  is the excitation light density,  $\Delta t_1$  is the pulse width of the excitation light,  $E_1$  is the excitation photon energy, and  $\alpha_1$  is the absorption coefficient  $\alpha$  for one-photon excitation at energy  $E_1$ , i.e.,  $\alpha_1 = \alpha(E_1)$ . For energies close to the band edge, the absorption coefficient becomes smaller for lower excitation energies. Therefore, the penetration depth ( $1/\alpha_1$ ) increases for lower energies, and the additional reabsorption results in the redshift of the PL spectrum.

To verify the above interpretation, we also performed the same experiment on the thin film sample. The 200-nm-thick film has negligible reabsorption due to its thickness, and thus no dependence on the excitation energy is expected. Five PL spectra for excitation near the band edge ( $E_1 = 3.08$ – $3.20$  eV) are shown with the red dots in Fig. 2(b). Strong scattering of the excitation laser appears in the PL spectra of thin films, but the spectra are sufficiently accurate for our purpose. For comparison, the PL spectrum for  $E_1 = 3.50$  eV is shown with the blue line. In contrast to the single crystal, the PL spectrum of the thin film is almost independent of the excitation energy. This result indicates that the PL line width of MAPbCl<sub>3</sub> is the homogeneous width rather than a result of broadening due to extrinsic factors like impurities or defects [40]. Moreover, we consider that the contribution of hot carrier emission is negligible for the PL, since the spectral shape exhibits no change in the peak energy and the high-energy tail even for higher excitation energies.

Now we investigate the behavior of the two-photon PL data. The PL spectra obtained from Fig. 1(b) for five different excitation energies ( $E_2 = 1.52$ – $1.64$  eV) are shown in Fig. 3(a). The photon energy is almost half of the band gap of the MAPbCl<sub>3</sub> single crystal. Therefore, two-photon absorption is the only possible excitation process. This two-photon PL exhibits a peak at 2.93 eV, which is strongly redshifted compared to the one-photon PL [Fig. 2(a)]. Figure 3(a) clearly shows that the two-photon PL spectral

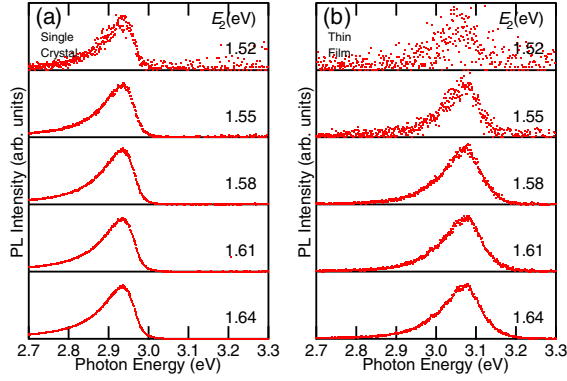


FIG. 3. The PL spectra for (a) the single crystal and (b) the thin film, under two-photon excitation with energies close to half of the band gap of MAPbCl<sub>3</sub>.

shape is independent of the excitation energy. Under two-photon excitation, the spatial distribution of the photoexcited carriers in depth can be written as [39]

$$n_2(z) = \frac{\beta_2 I_2^2 \Delta t_2}{2E_2(\beta_2 I_2 z + 1)^2} \sim \frac{\beta_2 I_2^2 \Delta t_2}{2E_2}. \quad (2)$$

By analogy with Eq. (1),  $I_2$ ,  $\Delta t_2$ , and  $E_2$  correspond to the excitation light density, the pulse width of the excitation light, and the excitation energy, respectively.  $\beta_2$  is the absorption coefficient for the two-photon excitation with energy  $E_2$ . Under two-photon excitation, the whole volume of the crystal is excited. Therefore, the contribution of the PL from inside the crystal is significant, and the observed PL is strongly influenced by reabsorption inside the sample. The 1- and 2-PL spectrum that includes reabsorption effects can be expressed with the following equation:

$$I_{k\text{-PL}}(E) \propto \gamma_{\text{spon}}(E) \int_0^L n_k(z) e^{-\alpha(E)z} dz. \quad (3)$$

The sample thickness is given with  $L$ , the emission energy is  $E$ , and  $\gamma_{\text{spon}}(E)$  is the spontaneous emission spectrum. Considering Eq. (3), the results shown in Fig. 3(a) indicate that the shape of the photocarrier distribution  $n_2(z)$  is unchanged at a different excitation energy  $E_2$ . In other words,  $n_2(z)$  has no depth dependence (which is possible only if  $\beta_2 I_2 z$  is much smaller than unity), and thus the approximation on the right side of Eq. (2) is valid; for each excitation energy, the carriers are excited uniformly throughout the sample.

To understand the influence of photon reabsorption, we compare the two-photon PL spectra obtained from the single crystal with those obtained from the thin film. The two-photon PL spectra obtained for five different excitation energies ( $E_2 = 1.52$ – $1.64$  eV) for the thin film are shown in Fig. 3(b). The spectral shape from the thin film is also independent of the excitation energy, but here the PL

peak energy (3.06 eV) remains the same as that observed for the one-photon PL spectra. Because the thin film has a limited thickness, both the one- and two-photon excitation excite the entire sample uniformly, resulting in almost the same photocarrier distribution.

Next, we extract the 1-PLE spectra from Fig. 1(a), i.e., a cut of the 2D image along the vertical axis, which enables the analysis of the strength of photon reabsorption for different energies. The PL intensities for five different detection energies as a function of the one-photon excitation energy  $E_1$  are shown in Fig. 4(a). The detection energies range from 2.99 to 3.11 eV with an increment of 30 meV, as indicated in the inset. Because of scattering of the excitation light, small sharp peaks can be observed when the excitation energy is equal to the detection energy.

The data evidence that, compared with the 1-PLE spectra for higher detection energies, the onset is shifted towards lower energies for the 1-PLE spectra at lower detection energies. This can be explained with a change in the photoexcited carrier distribution due to the change of the penetration depth for different excitation energies. A similar effect has been also observed in the transmission spectra of thick single crystals [20,29,41]. Furthermore, the data in Fig. 4(a) clearly support that the PLE peak observed at 3.1 eV vanishes if low detection energies are chosen. This can be explained analytically. The PLE intensity as a function of the one-photon excitation energy  $E_1$ , including effects from reabsorption on optically thick samples, can be written as [38]

$$I_{1\text{-PLE}}(E_0, E_1) \propto \frac{\alpha_1}{E_1(\alpha_0 + \alpha_1)}. \quad (4)$$

Here,  $\alpha_0$  is the absorption coefficient for one-photon excitation with a photon energy equal to the detection energy  $E_0$ , i.e.,  $\alpha_0 = \alpha(E_0)$ . When  $\alpha_1$  is much larger than  $\alpha_0$ , we have  $\alpha_1/(\alpha_0 + \alpha_1) \rightarrow 1$ , and thus the PL intensity  $I_{1\text{-PLE}}$  becomes independent of  $\alpha_1$ . Especially,  $\alpha_0$  is small in the low-energy detection region. Therefore, the 1-PLE spectrum saturates when the excitation energy is above that energy level. In this

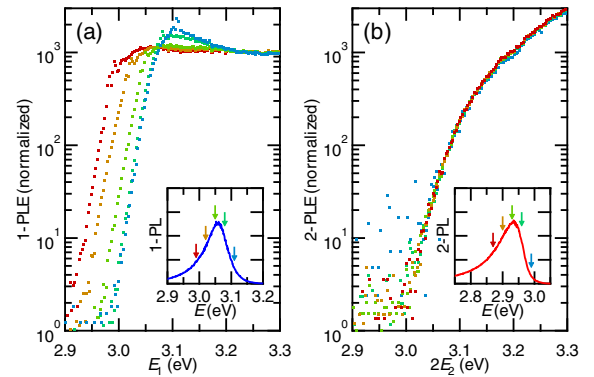


FIG. 4. (a) 1-PLE and (b) 2-PLE spectra of the MAPbCl<sub>3</sub> single crystal for different monitor wavelengths. The inset indicates the monitoring wavelength with a representative PL spectrum.



way, the large absorption in the direct transition semiconductors leads to a substantial change in the PLE spectra of samples with a certain thickness. Concurrently, this fact imposes to detect the PLE near this absorption peak in order to trace the strong excitonic absorption with the PLE technique.

Further comparison with the 2-PLE spectra for the MAPbCl<sub>3</sub> single crystal extracted from Fig. 1(b) clarifies the significant influence of reabsorption. Figure 4(b) shows the PL intensities for five different detection energies as a function of the two-photon excitation energy  $E_2$ . The detection energies range from 2.87 to 2.99 eV with an increment of 30 meV, as indicated with arrows in the inset. It is obvious that the shape of 2-PLE spectrum is independent of the detection energy; i.e., the 2-PLE signal intensity depends only on the two-photon absorption coefficient.

To determine the physical origin of the peak in the 1-PLE spectrum, the PL and PLE spectra for the MAPbCl<sub>3</sub> single crystal under one- and two-photon excitation conditions are compared in Fig. 5(a). The PL spectra are those for excitation energies  $E_1 = 3.50$  eV and  $E_2 = 1.75$  eV under one- and two-photon excitation, respectively. In order to obtain the 1-PLE spectrum near the absorption peak, the 1-PLE spectra recorded for the monitoring energies  $E_0 = 3.092$  and  $3.124$  eV were normalized at the center energy (3.108 eV) and plotted together. In this way, the sharp artifacts from the scattering of the excitation light can be removed easily. The 1-PLE spectrum depends on the monitoring energy  $E_0$  as shown in Fig. 4, but we confirmed that the PLE obtained by the integrated PL from the thin film is the same (see Supplemental Material [38]). Note that we can accurately measure the tail of the 1-PLE for MAPbCl<sub>3</sub> using single crystals, while it is difficult to measure the tail of the 1-PLE for thin films because of strong light scattering. The 1-PLE data correspond to the absorption spectrum and exhibit a peak structure at 3.11 eV. The corresponding PL spectrum for one-photon excitation

has a peak at 3.06 eV, meaning a Stokes shift of about 50 meV between PL and absorption. This value is as small as that of other halide perovskites [8,28,29]. The 2-PLE spectrum is that for the monitoring energy  $E_0 = 2.935$  eV. Compared to the 1-PLE spectrum, the 2-PLE spectrum has a weak onset without any peak structure. By considering the selection rule for band-to-band transitions, we can conclude that the peak in the 1-PLE spectrum originates from the  $1s$  exciton.

Now we discuss the excitation and detection-energy dependence of the PLE spectra with a model that accounts for the photocarrier distribution and reabsorption. This allows us to calculate the one- and two-photon absorption spectra, and the results for the MAPbCl<sub>3</sub> single crystal are shown in Fig. 5(b). The equations used are (the derivations are given in Supplemental Material [38])

$$\frac{\alpha(E_1)}{\alpha_0} = \frac{E_1 I_{1\text{-PLE}}(E_0, E_1)}{2E_0 I_{1\text{-PLE}}(E_0, E_0) - E_1 I_{1\text{-PLE}}(E_0, E_1)}, \quad (5)$$

$$\beta\left(\frac{E_1}{2}\right) = \frac{1}{\sqrt{2}} \frac{\alpha_0 \alpha_1}{\alpha_0 + \alpha_1} \frac{I_{2\text{-PLE}}(E_0, \frac{E_1}{2})/I_2^2}{I_{1\text{-PLE}}(E_0, E_1)/I_1}. \quad (6)$$

For simplification, we assumed  $E_1 = 2E_2$  and a peak value for the one-photon absorption coefficient  $\alpha_0 = 1.7 \times 10^6 \text{ cm}^{-1}$  from the literature [31]. First, we discuss the one-photon absorption spectrum [blue dots in Fig. 5(b)], with a sharp peak at 3.11 eV. By fitting the tail towards low energies with an exponential function, we obtain an Urbach energy of 11 meV. This value is smaller than the 23 meV reported for thin film samples [16], indicating that less defects are present in our single crystal sample. Furthermore, the one-photon absorption spectrum can be fitted well with the Elliott formula [42], which allowed us to calculate a band gap energy  $E_g$  of 3.149 eV and an exciton binding energy  $E_b = 41$  meV. Since the latter value is larger than the room-temperature energy ( $k_B T \sim 26$  meV), MAPbCl<sub>3</sub> has stable excitons even at room temperature. Recent investigations of the exciton binding energy in thin films and single crystals reported the values of 12–16 and 15–30 meV for MAPbI<sub>3</sub> and MAPbBr<sub>3</sub> single crystals, respectively [43–47]. When we compare these values with the 41 meV of this work, we can justify that our value is plausible. A highly interesting conclusion is that, although MAPbCl<sub>3</sub> is governed by excitonic responses, the highly efficient luminescence in combination with the sufficiently small Stokes shift in hybrid perovskites produces a strong reabsorption of excitonic PL.

Finally, we discuss the two-photon absorption spectrum [red dots in Fig. 5(b)]. Around 3 eV, this spectrum begins to increase gradually. Although the 2-PLE technique is sensitive and powerful to trace the excitonic or even higher order peaks [48,49], no peak structure is observed for the MAPbCl<sub>3</sub> single crystal. According to the selection rule for optical transitions involving two photons, the  $2p$  exciton is

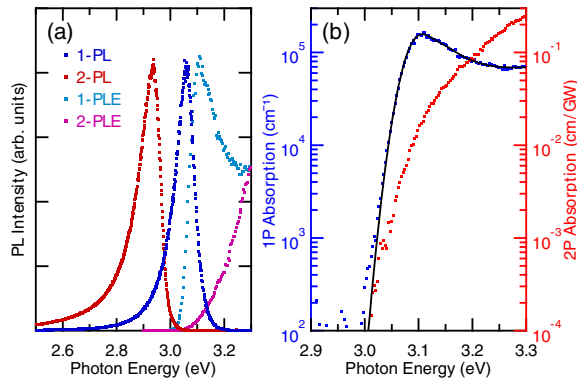


FIG. 5. (a) Comparison of PL and PLE spectra of the MAPbCl<sub>3</sub> single crystal for one- and two-photon excitation conditions. (b) The one-photon (blue) and two-photon (red) absorption spectra, as calculated from the PLE spectra. The continuous line is the fitting result using Elliott's formula.

allowed. However, compared to the room-temperature energy, the  $2p$  exciton lies energetically only slightly below the band edge (the estimated value is  $E_b/4$ –10 meV). Therefore, a clear excitonic structure was not observed for the two-photon absorption. To clarify the excitation energy dependence of the two-photon absorption spectrum, we employ the following scaling law for the two-photon absorption coefficient  $\beta$  [50]:

$$\beta(E) = \beta_0 \frac{(2E/E_g - 1)^{3/2}}{(2E/E_g)^5}. \quad (7)$$

By fitting the data with red dots in Fig. 5(b) with Eq. (7), we obtain  $\beta_0 = 21.8$  cm/GW and  $E_g = 3.143$  eV. The band gap energy agrees well with the one obtained from the one-photon absorption spectrum. Furthermore, the two-photon absorption coefficient  $\beta$  becomes 0.25 cm/GW at  $E = 1.65$  eV, which is smaller than that of other halide perovskites and also GaAs [50–52]. This result is consistent with the general trend that a wider band gap results in a smaller  $\beta$ .

In conclusion, we have grown a MAPbCl<sub>3</sub> single crystal and employed PLE measurements to investigate the optical and excitonic responses near the band edge. We experimentally verified that the influences of the photocarrier distribution and photon reabsorption have to be considered to explain the responses of the optically thick single crystal. A theoretical calculation supports our interpretation and allowed us to deduce accurate values for the band gap (3.15 eV) and exciton binding energy (41 meV) from the 1- and 2-PLE spectra of the single crystal. In MAPbCl<sub>3</sub>, the excitons are stable even at room temperature and thus govern the optical spectra and also the photon-recycling effects.

Part of this work was supported by CREST, JST (Grant No. JPMJCR16N3) and JSPS Research Fellowships for Young Scientists (Grant No. 17J07890).

\*Corresponding author.

kanemitsu@scl.kyoto-u.ac.jp

- [1] A. Kojima, K. Teshima, Y. Shirai, and T. Miyasaka, *J. Am. Chem. Soc.* **131**, 6050 (2009).
- [2] NREL, Research Cell Efficiency Records, <https://www.nrel.gov/pv/assets/images/efficiency-chart.png>.
- [3] M. Saliba, T. Matsui, K. Domanski, J.-Y. Seo, A. Ummadisingu, S. M. Zakeeruddin, J.-P. Correa-Baena, W. R. Tress, A. Abate, A. Hagfeldt, and M. Grätzel, *Science* **354**, 206 (2016).
- [4] A. Priyadarsh, L. J. Haur, P. Murray, D. Fu, S. Kulkarni, G. Xing, T. C. Sum, N. Mathews, and S. G. Mhaisalkar, *Energy Environ. Sci.* **9**, 3687 (2016).
- [5] S. D. Stranks, G. E. Eperon, G. Grancini, C. Menelaou, M. J. P. Alcocer, T. Leijtens, L. M. Herz, A. Petrozza, and H. J. Snaith, *Science* **342**, 341 (2013).
- [6] G. Xing, N. Mathews, S. Sun, S. S. Lim, Y. M. Lam, M. Grätzel, S. Mhaisalkar, and T. C. Sum, *Science* **342**, 344 (2013).
- [7] Y. Yamada, T. Nakamura, M. Endo, A. Wakamiya, and Y. Kanemitsu, *Appl. Phys. Express* **7**, 032302 (2014).
- [8] S. D. Wolf, J. Holovsky, S.-J. Moon, P. Löper, B. Niesen, M. Ledinsky, F.-J. Haug, J.-H. Yum, and C. Ballif, *J. Phys. Chem. Lett.* **5**, 1035 (2014).
- [9] Y. Yamada, T. Nakamura, M. Endo, A. Wakamiya, and Y. Kanemitsu, *J. Am. Chem. Soc.* **136**, 11610 (2014).
- [10] S. D. Stranks, V. M. Burlakov, T. Leijtens, J. M. Ball, A. Goriely, and H. J. Snaith, *Phys. Rev. Applied* **2**, 034007 (2014).
- [11] Q. Dong, Y. Fang, Y. Shao, P. Mulligan, J. Qiu, L. Cao, and J. Huang, *Science* **347**, 967 (2015).
- [12] H. Zhu, K. Miyata, Y. Fu, J. Wang, P. P. Joshi, D. Niesner, K. W. Williams, S. Jin, and X.-Y. Zhu, *Science* **353**, 1409 (2016).
- [13] A. Baumann, S. Vöth, P. Rieder, M. C. Heiber, K. Tvingstedt, and V. Dyakonov, *J. Phys. Chem. Lett.* **6**, 2350 (2015).
- [14] E. T. Hoke, D. J. Slotcavage, E. R. Dohner, A. R. Bowring, H. I. Karunadasa, and M. D. McGehee, *Chem. Sci.* **6**, 613 (2015).
- [15] R. Comin, G. Walters, E. S. Thibau, O. Voznyy, Z.-H. Lu, and E. H. Sargent, *J. Mater. Chem. C* **3**, 8839 (2015).
- [16] A. Sadhanala, S. Ahmad, B. Zhao, N. Giesbrecht, P. M. Pearce, F. Deschler, R. L. Z. Hoyer, K. C. Gödel, T. Bein, P. Docampo, S. E. Dutton, M. F. L. D. Volder, and R. H. Friend, *Nano Lett.* **15**, 6095 (2015).
- [17] Z. Xiao, R. A. Kerner, L. Zhao, N. L. Tran, K. M. Lee, T.-W. Koh, G. D. Scholes, and B. P. Rand, *Nat. Photonics* **11**, 108 (2017).
- [18] V. Adinolfi, O. Ouellette, M. I. Saidaminov, G. Walters, A. L. Abdelhady, O. M. Bakr, and E. H. Sargent, *Adv. Mater.* **28**, 7264 (2016).
- [19] E. Zheng, B. Yuh, G. A. Tosado, and Q. Yu, *J. Mater. Chem. C* **5**, 3796 (2017).
- [20] G. Maculan, A. D. Sheikh, A. L. Abdelhady, M. I. Saidaminov, M. A. Haque, B. Murali, E. Alarousu, O. F. Mohammed, T. Wu, and O. M. Bakr, *J. Phys. Chem. Lett.* **6**, 3781 (2015).
- [21] F. Zheng, L. Z. Tan, S. Liu, and A. M. Rappe, *Nano Lett.* **15**, 7794 (2015).
- [22] E. M. Hutter, M. C. Gélvez-Rueda, A. Osherov, V. Bulović, F. C. Grozema, S. D. Stranks, and T. J. Savenije, *Nat. Mater.* **16**, 115 (2017).
- [23] V. D’Innocenzo, A. R. S. Kandada, M. D. Bastiani, M. Gandini, and A. Petrozza, *J. Am. Chem. Soc.* **136**, 17730 (2014).
- [24] Y. Tian and I. G. Scheglykin, *J. Phys. Chem. Lett.* **6**, 3466 (2015).
- [25] M. Shirayama, H. Kadowaki, T. Miyadera, T. Sugita, M. Tamakoshi, M. Kato, T. Fujiseki, D. Murata, S. Hara, T. N. Murakami, S. Fujimoto, M. Chikamatsu, and H. Fujiwara, *Phys. Rev. Applied* **5**, 014012 (2016).
- [26] Y. Kanemitsu, *J. Mater. Chem. C* **5**, 3427 (2017).
- [27] Y. Yamada, T. Yamada, and Y. Kanemitsu, *Bull. Chem. Soc. Jpn.* **90**, 1129 (2017).
- [28] Y. Yamada, T. Yamada, L. Q. Phuong, N. Maruyama, H. Nishimura, A. Wakamiya, Y. Murata, and Y. Kanemitsu, *J. Am. Chem. Soc.* **137**, 10456 (2015).
- [29] T. Yamada, Y. Yamada, H. Nishimura, Y. Nakaike, A. Wakamiya, Y. Murata, and Y. Kanemitsu, *Adv. Electron. Mater.* **2**, 1500290 (2016).

- [30] T. Yamada, Y. Yamada, Y. Nakaike, A. Wakamiya, and Y. Kanemitsu, *Phys. Rev. Applied* **7**, 014001 (2017).
- [31] M. Kato, T. Fujiseki, T. Miyadera, T. Sugita, S. Fujimoto, M. Tamakoshi, M. Chikamatsu, and H. Fujiwara, *J. Appl. Phys.* **121**, 115501 (2017).
- [32] J. F. Muth, J. H. Lee, I. K. Shmagin, R. M. Kolbas, H. C. Casey Jr., B. P. Keller, U. K. Mishra, and S. P. DenBaars, *Appl. Phys. Lett.* **71**, 2572 (1997).
- [33] F. Staub, T. Kirchartz, K. Bittkau, and U. Rau, *J. Phys. Chem. Lett.* **8**, 5084 (2017).
- [34] L. M. Pazos-Outón, M. Szumilo, R. Lamboll, J. M. Richter, M. Crespo-Quesada, M. Abdi-Jalebi, H. J. Beeson, M. Vručinić, M. Alsari, H. J. Snaith, B. Ehrler, R. H. Friend, and F. Deschler, *Science* **351**, 1430 (2016).
- [35] J. M. Richer, M. Abdi-Jalebi, A. Sadhanala, M. Tabachnyk, J. P. H. Rivett, L. M. Pazos-Outón, K. C. Gödel, M. Price, F. Deschler, and R. H. Friend, *Nat. Commun.* **7**, 13941 (2016).
- [36] T. Kirchartz, F. Staub, and U. Rau, *ACS Energy Lett.* **1**, 731 (2016).
- [37] Y. Fang, H. Wei, Q. Dong, and J. Huang, *Nat. Commun.* **8**, 14417 (2017).
- [38] See Supplemental Material at <http://link.aps.org/supplemental/10.1103/PhysRevLett.120.057404> for the sample preparation, experimental setup, reabsorption model for PLE spectra, origin of the asymmetric intrinsic emission spectrum, and comparison of PLE spectra obtained from the single crystal and the thin film.
- [39] N. Naka, T. Kitamura, J. Omachi, and M. Kuwata-Gonokami, *Phys. Status Solidi (b)* **245**, 2676 (2008).
- [40] C. Wehrenfennig, M. Liu, H. J. Snaith, M. B. Johnston, and L. M. Herz, *J. Phys. Chem. Lett.* **5**, 1300 (2014).
- [41] D. Shi, V. Adinolfi, R. Comin, M. Yuan, E. Alarousu, A. Buin, Y. Chen, S. Hoogland, A. Rothenberger, K. Katsiev, Y. Losovyj, X. Zhang, P. A. Dowben, O. F. Mohammed, E. H. Sargent, and O. M. Bakr, *Science* **347**, 519 (2015).
- [42] R. J. Elliott, *Phys. Rev.* **108**, 1384 (1957).
- [43] L. Q. Phuong, Y. Nakaike, A. Wakamiya, and Y. Kanemitsu, *J. Phys. Chem. Lett.* **7**, 4905 (2016).
- [44] Z. Yang, A. Surrente, K. Galkowski, N. Bruyant, D. K. Maude, A. A. Haghighirad, H. J. Snaith, P. Plochocka, and R. J. Nicholas, *J. Phys. Chem. Lett.* **8**, 1851 (2017).
- [45] H. Kunugida, Y. Kiyota, Y. Udagawa, Y. Takeoka, Y. Nakamura, J. Sano, T. Matsushita, T. Kondo, and K. Ema, *Jpn. J. Appl. Phys.* **55**, 060304 (2016).
- [46] J. Tilchin, D. N. Dirin, G. I. Maikov, A. Sashchiuk, M. V. Kovalenko, and E. Lifshitz, *ACS Nano* **10**, 6363 (2016).
- [47] D. Niesner, O. Schuster, M. Wilhelm, I. Levchuk, A. Osvet, S. Shrestha, M. Batentschuk, C. Brabec, and T. Fauster, *Phys. Rev. B* **95**, 075207 (2017).
- [48] F. Wang, G. Dukovic, L. E. Brus, and T. F. Heinz, *Science* **308**, 838 (2005).
- [49] Y. Kimoto, M. Okano, and Y. Kanemitsu, *Phys. Rev. B* **87**, 195416 (2013).
- [50] G. Walters, B. R. Sutherland, S. Hoogland, D. Shi, R. Comin, D. P. Sellan, O. M. Bakr, and E. H. Sargent, *ACS Nano* **9**, 9340 (2015).
- [51] B. S. Kalanoor, L. Gouda, R. Gottesman, S. Tirosh, E. Haltzi, A. Zaban, and Y. R. Tischler, *ACS Photonics* **3**, 361 (2016).
- [52] R. Zhang, J. Fan, X. Zhang, H. Yu, H. Zhang, Y. Mai, T. Xu, J. Wang, and H. J. Snaith, *ACS Photonics* **3**, 371 (2016).